Modern armour configurations against 14.5 mm AP

Diederen, A.M.[1], Broos, J.P.F.[1], Peijen, M.C.P.[2]

[1] TNO Prins Maurits Laboratory, P.O. Box 45, NL-2280 AA Rijswijk, The Netherlands
[2] Royal Netherlands Army, Directorate of Materiel, P.O. Box 90822, NL-2509 LV The Hague

Abstract

This paper presents the experimentally established ballistic resistance of armour configurations with modern ballistic materials against Russian 14.5 mm AP-I B32 (steel core) ammunition. The materials involved are ultra hard / high-hardness steel, aluminium, titanium, ceramics and composites. Tests are conducted at both 0º and 60º NATO impact angles. For a number of armour configurations the ballistic limit velocities such as the V99 are established using the Kneubuehl method. These threshold velocities correspond with a certain probability of stopping the ammunition (99% for V99). The different armour configurations can be compared using a single graph per stopping probability (e.g. 99%) which shows the areal density of the tested armour configurations against the minimum shooting distance for which the 14.5 mm AP ammunition will be stopped with the probability indicated.

1. Background

The current inventory of military vehicles of The Netherlands as well as of most European countries largely originates from the period of the Cold War, both as to procurement and especially as to development. For peace operations however the threat for passengers and crew has changed dramatically. Vehicles with a well-protected frontal arc or vehicles, which before would operate behind the frontlines, are now exposed to threats from around (including from behind), from above and from beneath. Examples are snipers, mines (a/o. horizontal effect mines) and handheld anti-tank weapons. Moreover, both politics and the public accept own victims during peace operations even less than would be the case when more direct national interests would be at stake. For this reason the protection of passengers and crew of vehicles, especially for the lighter vehicles, often has to be changed drastically. At the same time the accompanying increase in weight has to be limited to prevent the need for adapting parts like the engine, driveline and suspension which would make the vehicle even heavier.
At the same time the total spectrum of threats against armoured vehicles is very extensive and diverse. The number of artillery-delivered (canons, rockets and mortars) ‘high performance’ ammunition types alone will increase from 18 to 94 during the next 10 years for the types that will be developed outside the United States [1]. The number of ATGMs (Anti-Tank Guided Missile) will increase from 43 to 68 during the same period [1]. It is clear that the arms race between ammunition and armour is all but finished. In order to limit the weight increase associated with the necessary levels of armour protection there is a strong need for ballistic materials with a high mass

efficiency (see definition in Appendix A), often leading to the application of lightweight armour materials.
It is clear that there is great demand for lightweight armour systems: for upgrading existing vehicles, for add-on armour for both existing and new vehicles and for designing new vehicles, bearing both existing and emerging new threats in mind.

2. Introduction

We have chosen to test armour configurations mainly based on aluminium armour representing the hull of a light to medium armoured vehicle. Aluminium has been chosen because it offers sufficient structural stiffness for these types of vehicles and because (depending on the threat and the aluminium type) aluminium armour has a slightly higher mass efficiency than RHA (Rolled Homogeneous Armour). See Appendix A for the definition of mass efficiency. Besides aluminium, also titanium base armour has been used because of its relatively high mass efficiency (1.5 to 1.8 against kinetic energy ammunition according to several sources) combined with its suitability to be used as a hull material with sufficient structural stiffness despite low areal densities.
Among the chosen armour configurations, a thin spall-liner has been used together with titanium base armour for two reasons. The first reason is that titanium shows considerably more spalling than aluminium armour, so a spall-liner is called for to protect the vehicle crew. The second reason is to validate and quantify the effect of a thin spall-liner increasing the threshold velocity of an armour configuration against a specific threat, given that the armour is almost balanced against that specific threat.

In order to investigate the ballistic protection of as many modern and new materials as possible for the given budget, besides normal impact only one oblique impact angle has been chosen: 60º NATO. If one can only choose one oblique impact angle, this angle is considered to be the most representative for the vertical angle between the shooting line and the frontal (sloped) vehicle armour as well as for oblique impact of the vehicle side armour when hit from the terrain in front of the vehicle. It is always possible to estimate the influence of other impact angles afterwards without the need for additional experiments by performing computer simulations, e.g. with the hydrocode Autodyn. The experimental results already available will hereby act as validation for these computer simulations.

For the experiments covered by this paper which constitutes the first series of experiments in a multi-year research project, the Russian 14.5 mm AP-I B32 (steel core) ammunition has been chosen. This represents the upper part of the threat spectrum for kinetic energy projectiles from non-regular opposing forces. This type of ammunition and the weapons to use it are widely spread (40+ countries) and relatively easy to produce.
The armour configurations will be compared to one another based on their V99 (99% stopping probability) because this is much closer to real protection requirements than for instance the V50 (50% stopping probability). As will be shown in this paper, the sequence of performance of armour configurations is different when based on the V99 instead of the V50.

3. Armour configurations

All armour configurations consist of aluminium or titanium base armour with a hard outer layer of other materials. All metallic outer layers are spaced from the aluminium or titanium, the ceramic containing outer layers are adhesively bonded to the (aluminium) base armour.
Table 1 gives an overview of the applied armour configurations, which are depicted in Appendix B.

Table 1

Armour config.	Impact angle	1st outer layer	airgap	2nd outer layer	airgap	Base armour	Liner
1	0º	SPS-43	yes	SPS-43	yes	Al 5083 H321	-
2	0º	ARMOX-600S	yes	ARMOX-600S	yes	Al 5083 H321	-
3	0º	ARMOX-600S	yes	-	-	Al 5083 H321	-
4	60º	SPS-43	yes	-	-	Al 5083 H321	-
5	60º	ARMOX-600S	yes	-	-	Al 5083 H321	-
6	0º	ARMOX-600S	yes	-	-	Ti-6Al-4V	-
7	0º	ARMOX-600S	yes	-	-	Ti-6Al-4V	Dyneema
8	60º	SPS-43	yes	-	-	Ti-6Al-4V	-
9	0º	LIBA	-	-	-	Al 5083 H321	-
10	60º	LIBA	-	-	-	Al 5083 H321	-
11	0º	MARS-300 perf	-	MARS-300 perf	yes	Al 5083 H321	-
12	60º	MARS-300 perf	yes	-	-	Al 5083 H321	-
13	0º	DIMOX-AS	-	-	-	Al 5083 H321	-

The lateral target dimensions are 500 x 500 mm, except for the Dyneema spall-liners that have lateral dimensions of 460 x 460 mm. The (apparent) density 'ρ' (see text below) of the armour plates has been determined by measuring the dimensions and weighing the plates.

Three types of very hard steel with a Brinell hardness of around 500 HB (SPS-43) and around 600 HB (ARMOX-600S and MARS-300 perforated) have been chosen:
- ARMOX-600S, manufactured by Swedish Steel, $\rho = 7.84$ g/cm^3.
- SPS-43, manufactured by Special Materials, St. Petersburg, Russia, $\rho = 7.63$ to 7.70 g/cm^3, dependent on plate thickness.
- MARS-300 perforated, manufactured by Creusot-Loire of France, $\rho = 4.09$ to 5.25 g/cm^3, dependent on the hole size which varies with the plate thickness.

For titanium, the customary alloy Ti-6Al-4V has been chosen. The titanium armour plates for target configurations 6, 7 and 8 (see table 1) have been cut from a large plate of 'Tikrutan LT31' with a Brinell hardness of around 300 HB, manufactured by Deutsche Titan of Germany. The measured density is 4.45 g/cm^3.

LIBA (Light Improved Ballistic Armour) consists of very hard ceramic pellets in a matrix of a polyurethane rubber / resin mixture. It is an Israeli invention [2] and is marketed for Europe by Ten Cate Advanced Composites of The Netherlands.

The LIBA was clamped directly to the aluminium base armour using screw clamps and quick-acting clamps. The measured density is 3.00 g/cm^3 and 2.97 g/cm^3 for the normal and oblique LIBA target plates respectively.

DIMOX-AS Type 112 is a so-called CMC (Ceramic Matrix Composite) and consists of SiC (siliciumcarbide) particles reinforcing a matrix of Al_2O_3 (alumina) and an interconnected network of aluminium alloy. This CMC combines (part of) the very high hardness of ceramic armour with (part of) the multihit capacity of aluminium armour. Manufacturer is Lanxide Armor Products, Newark, United States of America. The measured density is 3.25 g/cm^3.
The DIMOX tiles (lateral dimensions of 100 x 100 mm) are attached to the aluminium base armour using the flexible polyurethane adhesive SIKAFLEX 228. To save material cost, each DIMOX tile is laterally confined by the much cheaper Al_2O_3 tiles of similar thickness. The tile pattern is like a brick wall, see figure 1.

The Dyneema polyethylene fibre spall-liner, type UD-HB2, is manufactured by DSM High Performance Fibers of The Netherlands. The measured density is 0.92 g/cm^3.
The Dyneema is mounted on the titanium base armour of configuration 7 by means of 5 bolts (4 at the corners and one at the centre).

The aluminium base armour (Al 5083 H321) has a Brinell hardness of around 95 HB and a density of 2.65 g/cm^3. Most aluminium armour plates were manufactured by British Aluminium.

Apart from the armour configurations mentioned in table 1 also target configurations comprising SiC tiles and Al_2O_3 tiles on aluminium Al 7039 base armour have been tested. However, insufficient experiments have been performed so far to establish their threshold velocities.
Both SiC and Al_2O_3 tiles (lateral dimensions of 100 x 100 mm) are attached to the aluminium base armour using the flexible polyurethane adhesive SIKAFLEX 228. Again to save material cost, each SiC tile is laterally confined by Al_2O_3 tiles of equal thickness, see the tile pattern of figure 1. The lateral dimensions of the underlying aluminium base armour (ρ=2.74 g/cm^3) are 800 x 300 mm. For SiC ρ=3.12 g/cm^3, for Al_2O_3 (96% alumina content) ρ=3.69 g/cm^3. The ceramic tiles were manufactured by ETEC of Germany.

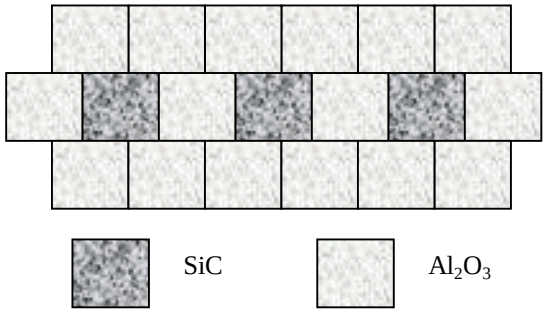

Fig. 1. Tile pattern for SiC tiles, confined by Al_2O_3 tiles.

4. Test set-up

The targets are mounted on a frame (0º frame or 60º frame) using screw clamps and quick-acting clamps. The armour plates are spaced from one another using square tubular sections at the perimeter of the armour plates. The weapon is placed at a fixed position; the target is shifted before each shot so an undamaged part can be impacted. The distance between weapon and target is 28.7 meters. The impact velocity of the projectile is registered just in front of the target by means of 2 light screens (see figure 2). For a number of experiments high-speed photography recordings have been made using an Imacon 468 camera (see figure 2).

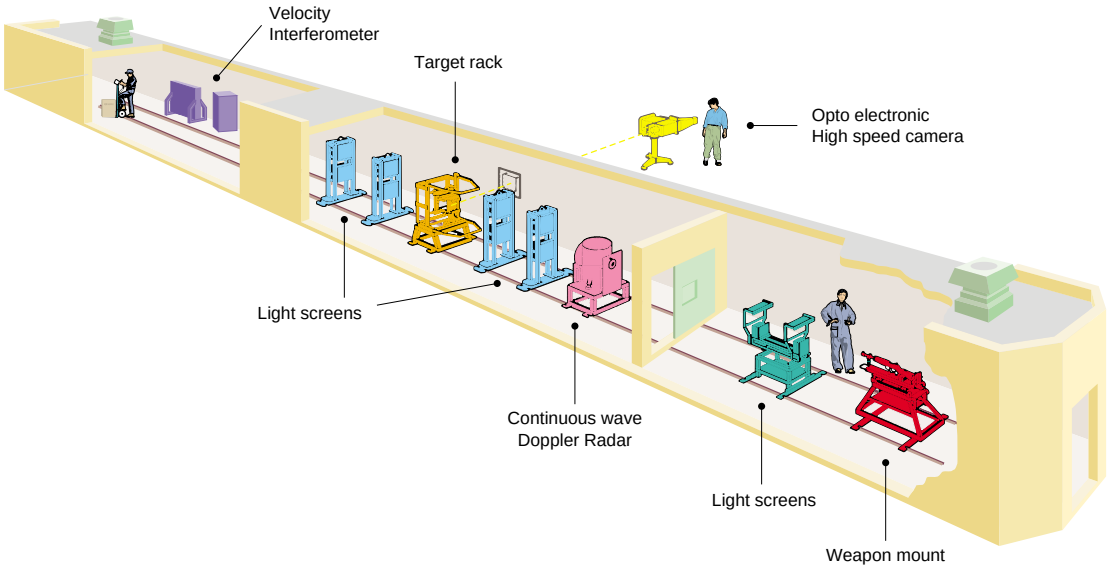

Fig. 2. Small-calibre test range at TNO Prins Maurits Laboratory.

In order to determine the threshold velocity (V50, V90, and so on) as a function of the impact velocity, a number of shots have to perforate the target and a number of shots have to be stopped by the target. For this reason for a large number of shots the amount of gunpowder in the cartridge has to be diminished to establish a lower impact velocity (corresponding with a larger shooting distance). For a limited number of shots the amount of gunpowder has been slightly increased to establish a sufficient number of perforations.

5. Kneubuehl method

The threshold velocities (V50, V90, and so on) are determined according to the Kneubuehl method [3]. This requires a minimum number of 12 shots. The difference between this method and the V50-determination according to STANAG 2920 is that the Kneubuehl method takes the standard deviation into account. By so doing, the threshold velocity is determined as a function of impact velocity instead of determining only one specific threshold velocity (V50: 50% stopping probability). By using the Kneubuehl method, not only the V50 is established but also the sensitivity for decreasing or increasing the impact velocity (shooting distance). This is important, because an armour which is in favour of another armour based only on the V50 (see solid line opposed to dashed line in example of figure 3) can perform worse than the

other armour at a lower impact velocity (in this example a lower V90 than the other armour).

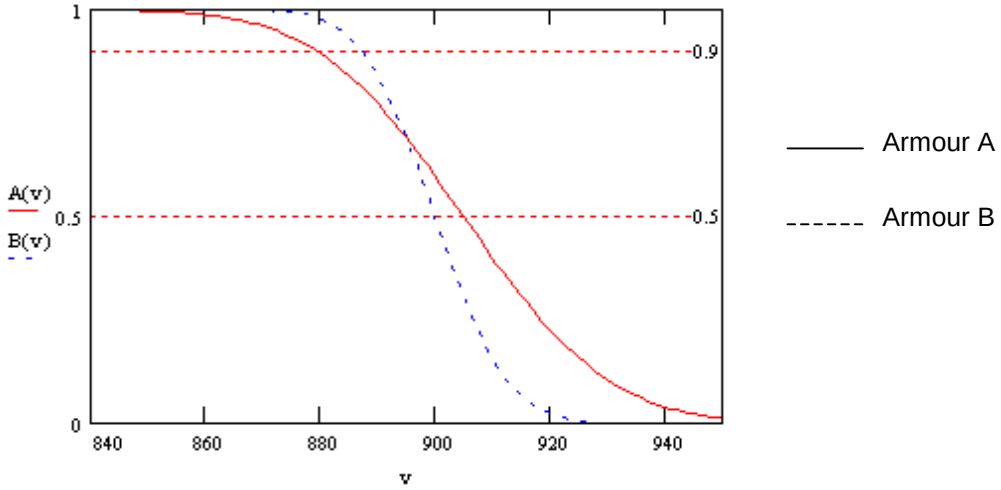

Fig. 3. Example of threshold velocities as a function of impact velocity (vertical axis: stopping probability; horizontal axis: impact velocity).

Given the V50 and the standard deviation 'σ' of an armour configuration, the stopping probability 'P' for any impact velocity 'V_t' can be estimated using the formula [3]:

$$P(V_t) = 1 - \frac{1}{\sqrt{2\pi}\cdot\sigma}\int_{-\infty}^{V_t} e^{-\frac{1}{2}\left(\frac{V-V50}{\sigma}\right)^2} dV$$

6. Results

For each armour configuration except no. 13 (see table 1) 12 to 20 shots have been performed (12 is the required minimum for the Kneubuehl method). The impact velocities have been chosen in such a way that both stops and perforations have been realised so that the threshold velocities (see table 2) could be established. The V50 corresponds with an estimated stopping probability of 50%, the V90 corresponds with an estimated stopping probability of 90%, and so on. The areal densities (kg/m^2) are given relative to RHA required to stop the threat (14.5 mm AP-I B32).
For target configuration 13 only a V50 could be established using the method according to STANAG 2920.

Table 2

Armour config.	Impact angle	V50 [m/sec]	V90 [m/sec]	V99 [m/sec]	Standard deviation [m/sec]	Areal density relative to RHA (RHA=100%)
1	0º	899	872	850	21.1	60.0
2	0º	833	782	741	39.8	52.2
3	0º	906	877	853	22.7	58.5
4	60º	788	773	761	11.2	51.1
5	60º	909	889	873	15.5	61.1
6	0º	905	889	875	12.8	50.4
7	0º	994	980	969	10.7	52.0
8	60º	880	856	836	18.7	49.8
9	0º	878	874	872	2.5	44.1
10	60º	933	863	805	55.2	55.5
11	0º	936	924	913	9.7	56.6
12	60º	904	856	816	38.1	55.1
13	0º	851 *)			14 *)	38.1

*) established according to STANAG 2920

Figure 4 is a graphical representation of the results (V50 and V90) for normal impact. It shows the influence of the standard deviation or spread in the results on the relative performance of the armour configurations.

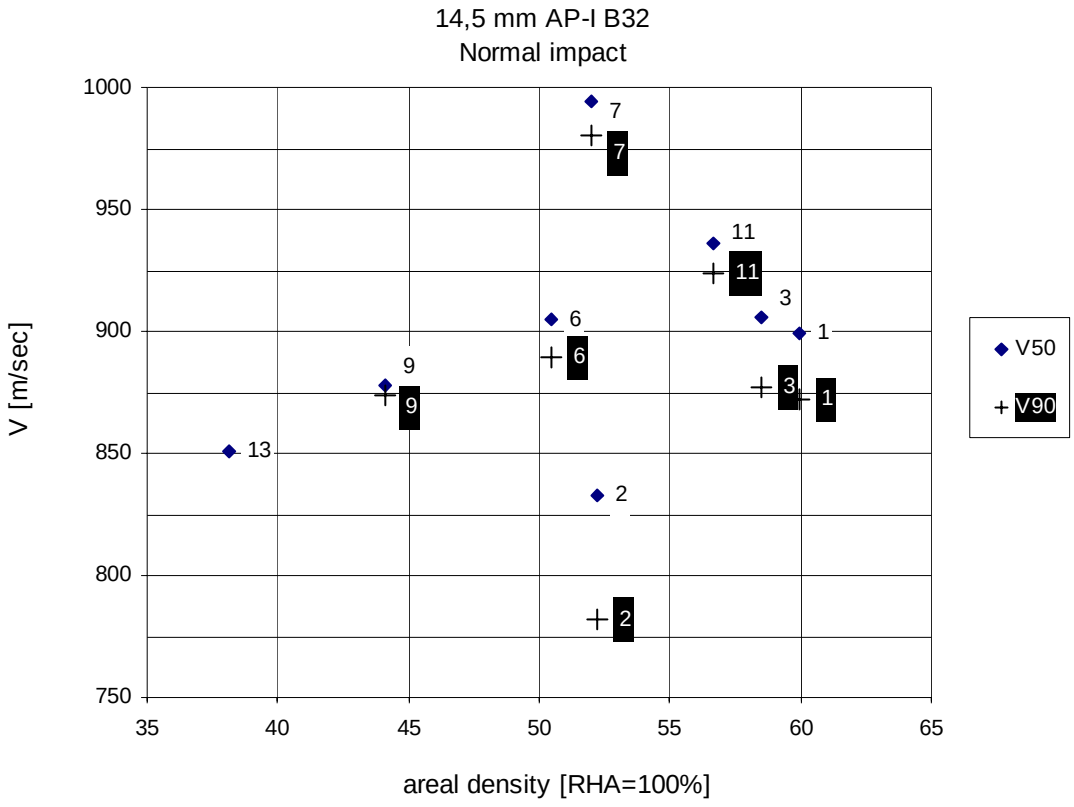

Fig.4. V50 and V90 as a function of areal density.

Figure 5 is another way of representing the results from table 2, using the formula according to Kneubuehl (see chapter 5) and showing that the relative performance of armour configurations is different when based on the V99 instead of the V50. A clear example is the marked difference between the LIBA targets for normal impact (armour configuration 9) and for oblique impact (armour configuration 10). The V50 for armour configuration 10 is higher than for armour configuration 9, but due to the large spread in experimental results (the large standard deviation) its V99 is lower than for armour configuration 9.

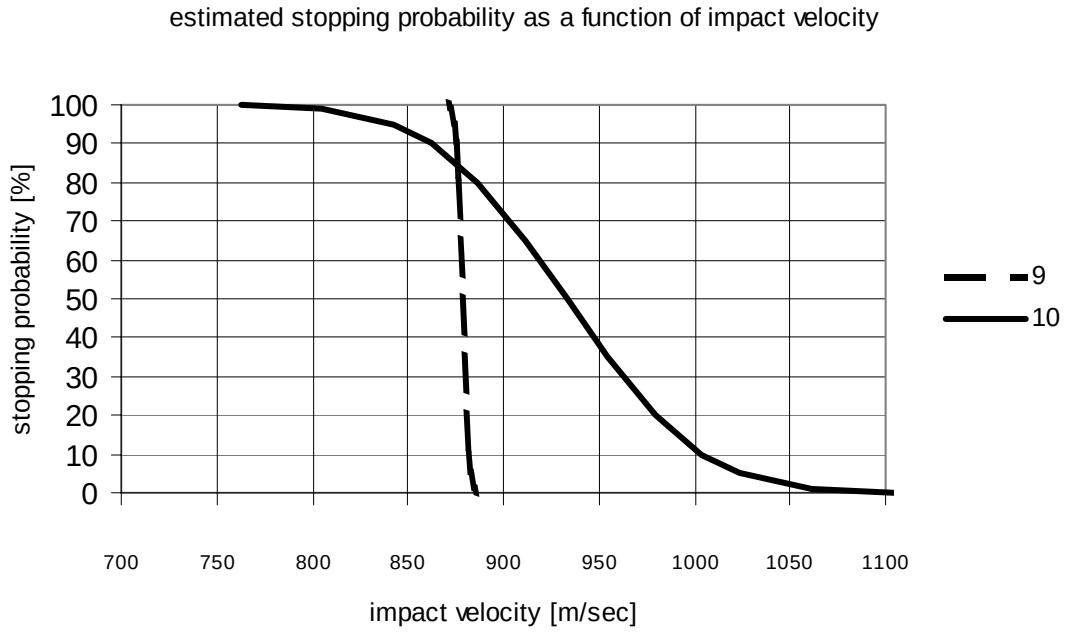

Fig.5. Estimated stopping probability as a function of impact velocity.

Figure 6 gives the required areal density (relative to RHA) for the armour configurations impacted at 0º NATO to realise an estimated stopping probability of 99%. Figure 7 gives these results for the armour configurations impacted at 60º NATO. At the right of figures 6 and 7 the shooting distance corresponding with the impact velocity along the vertical axis is given, based on MIL-Std-662E, Issue 94-04.

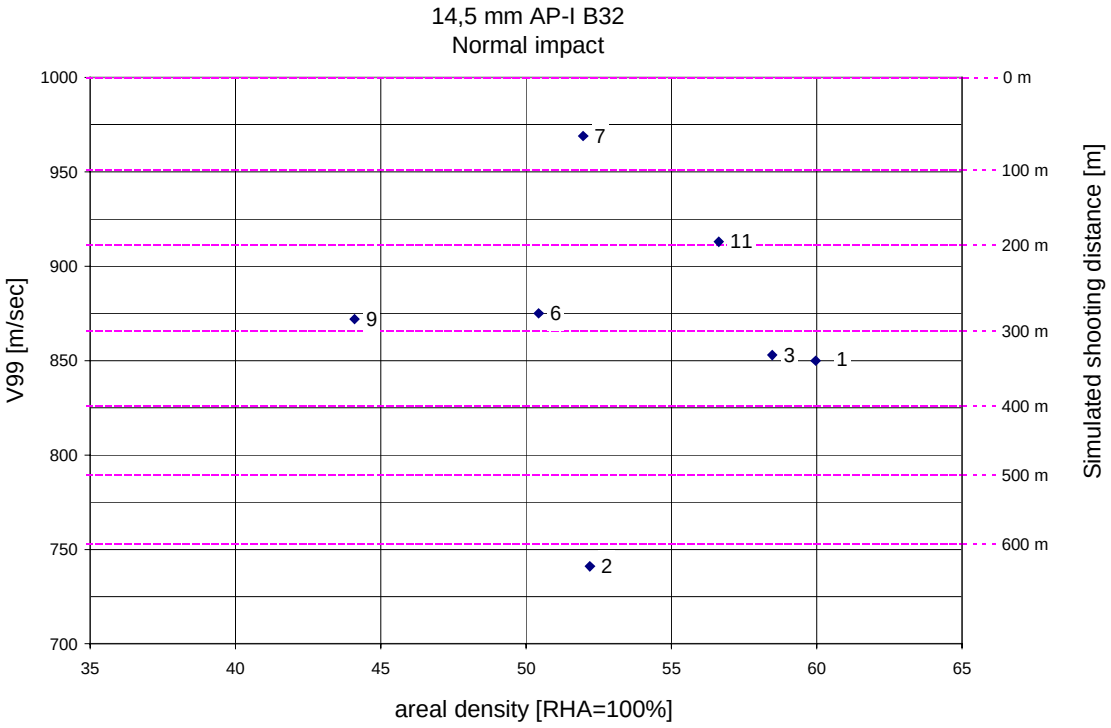

Fig. 6. Required areal densities for an estimated stopping probability of 99%, 0º NATO impact.

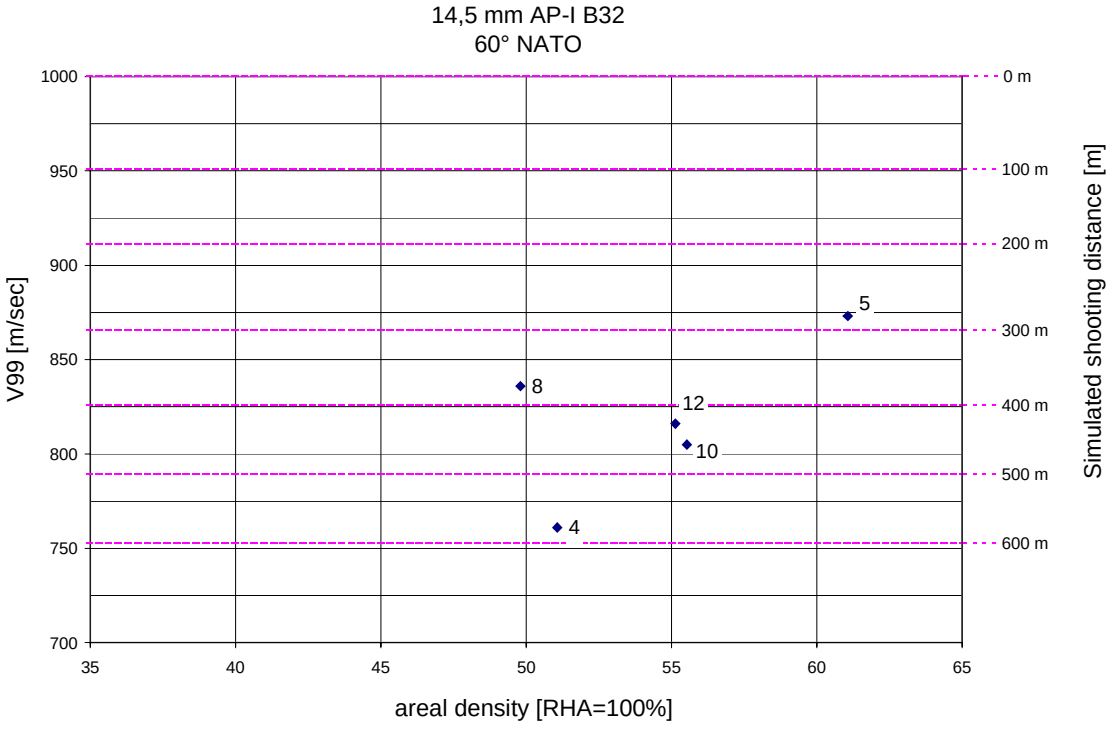

Fig. 7. Required areal densities for an estimated stopping probability of 99%, 60º NATO impact.

Figure 6 shows a decrease in areal density of the armour configurations from very hard steel (1, 2 and 3) and perforated very hard steel (11) via very hard steel in front of titanium base armour (6 and 7) to ceramic pellets in a rubber matrix (9) as outer layer. For armour configuration 13 no V99 has been established, but figure 4 shows that this armour configuration (ceramic matrix composite as outer layer) has a favourable ratio of threshold velocity (V50) and areal density.

Based on figure 6 and looking only at the ballistic protection, it can be concluded that armour configurations 11, 7, 6 and 9 are clearly preferable to armour configurations 1 and 3 because of their higher V99s at lower areal densities.
Looking at armour configuration 2 compared to 1 and 3 (all very hard steel plus aluminium) one could sketch an estimated trendline from 2 to 1 or 3 showing the effect of increasing the V99 with increasing areal density of these armour configurations of the same kind. So armour configuration 2 is not necessarily better or worse than armour configurations 1 or 3. The same consideration is valid for armour configuration 13 in figure 4. By increasing its areal density the V50 of armour configuration 13 may well match the V50 of armour configuration 9 and still possess a lower areal density.
In the ideal situation with sufficient funding and capacity, one would procure additional armour materials and perform additional tests. Alternatively, a trendline showing the increase in V50 or V99 at higher areal densities can be estimated by computer simulations, based on the experimental results already available as a reference.

Figure 7 shows the results for oblique impact (60º NATO). Bearing in mind that a certain armour configuration will have a higher V99 when its thickness and areal density is increased, armour configurations 4, 10, 12 and 5 have a ratio between V99 and areal density not too much different from one another. So only a clear distinction can be made between armour configuration 8 (very hard steel plus titanium) with the best ratio of V99 and areal density, and the other armour configurations (4, 10, 12 and 5).

For normal impact the areal density ranges from less than 45% (ceramic pellets in a rubber matrix, backed by aluminium) to around 60% (very hard steel plus aluminium) of the areal density of RHA required to stop the threat (14.5 mm AP-I B32). For the target configurations tested at 60º NATO impact angle, the areal density ranges from around 50% (very hard steel plus titanium) to over 60% (very hard steel plus aluminium).

SPS-43 and ARMOX-600S (armour configurations 1 to 5)
Some of the very hard SPS-43 steel armour plates (around 500 HB) exhibit cracking, both for the 0º NATO and the 60º NATO impact angle experiments. The clamping of these plates at their corners may cause this, but the even harder ARMOX-600S steel armour plates (around 600 HB) did not crack a single time. It should be noted however that the SPS-43 plates were much thinner than the used ARMOX-600S plates.

Figure 8 shows the backside of an SPS-43 steel armour plate of armour configuration 1, figure 9 shows the backside of an ARMOX-600S steel armour plate of armour configuration 3.

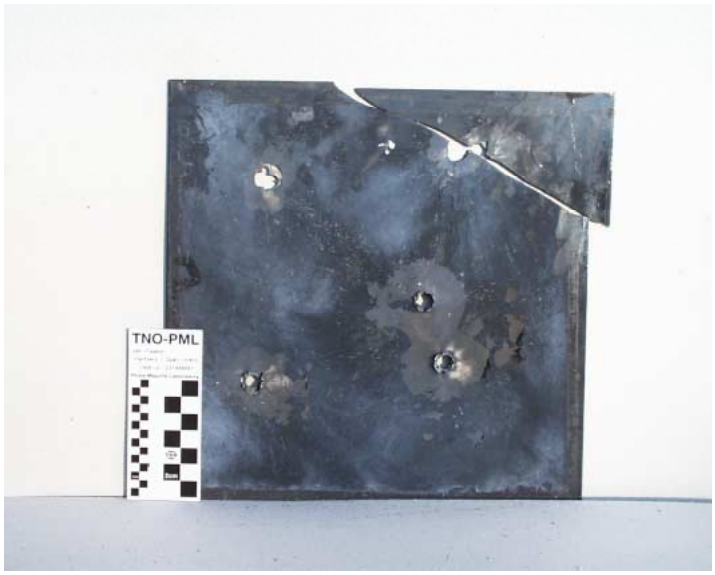

Fig.8. Crack in corner of SPS-43 steel armour plate (armour configuration 1).

Fig.9. Backside of ARMOX-600S steel armour plate (armour configuration 3).

MARS-300 perforated (armour configurations 11 and 12)

Perforated armour is very hard steel armour having a regular pattern of circular holes. In this way the (apparent) density is reduced (up to around 50%) and cracking due to a hit is prevented because a crack will not cross the perforations.

Figure 10 presents an Imacon recording of target 11 at normal impact (2 different layers of perforated armour directly on top of one another, spaced from an aluminium base armour), showing the projectile parts perforating the aluminium angled from the shooting line. The projectile moves from left to right. The incendiary tip of the projectile causes the bright flash in the Imacon recording.
Figures 11 to 13 show pictures of the damaged plates of armour configuration 11, in sequence of being penetrated by the projectile. Figures 14 and 15 show similar pictures for armour configuration 12 (one perforated armour plate similar to the second perforated armour plate of target 11, spaced from a thin aluminium base armour), impacted at 60º NATO.

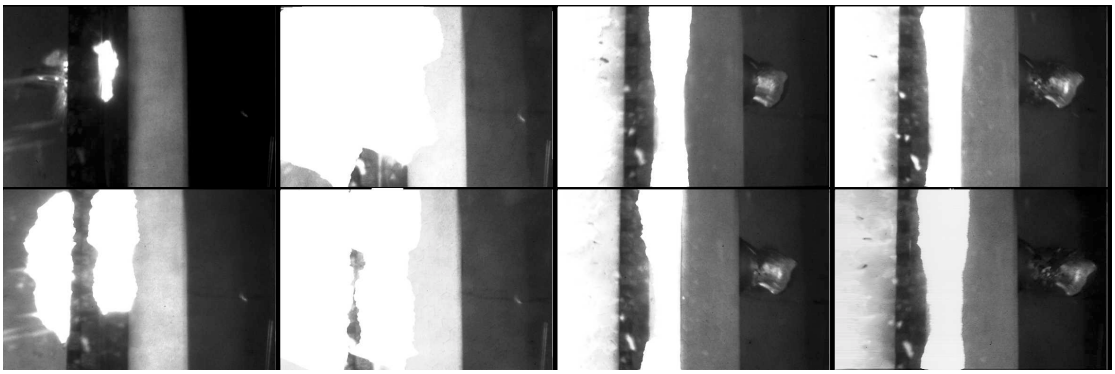

1	3	5	7
2	4	6	8

Fig.10. Imacon recording of target 11 (2 different plates of MARS-300 perforated / airgap / aluminium), impact velocity 1015 m/sec, timeframe per recording 27 μsec except 127 μsec between 4th and 5th frame, exposure 1 μsec.

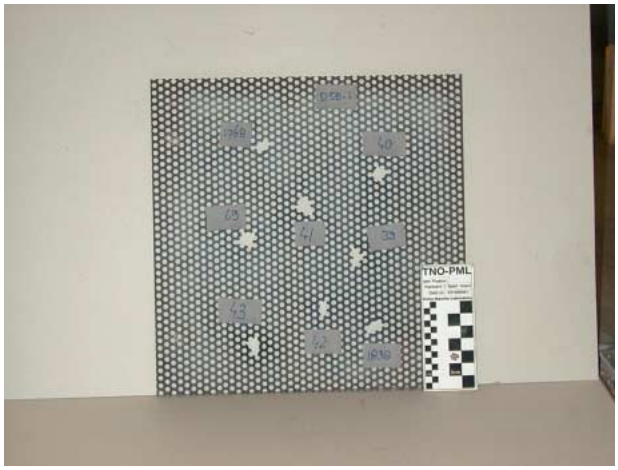

Fig. 11. Frontside of a front plate of MARS-300 perforated, armour configuration 11.

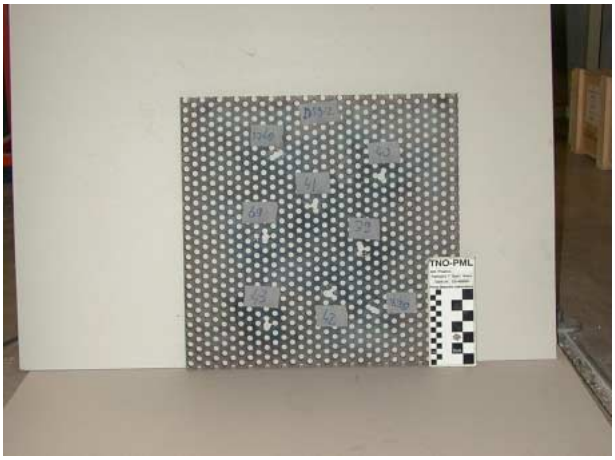

Fig. 12. Frontside of a rear plate of MARS-300 perforated, armour configuration 11.

Fig. 13. Backside of an aluminium plate of armour configuration 11.

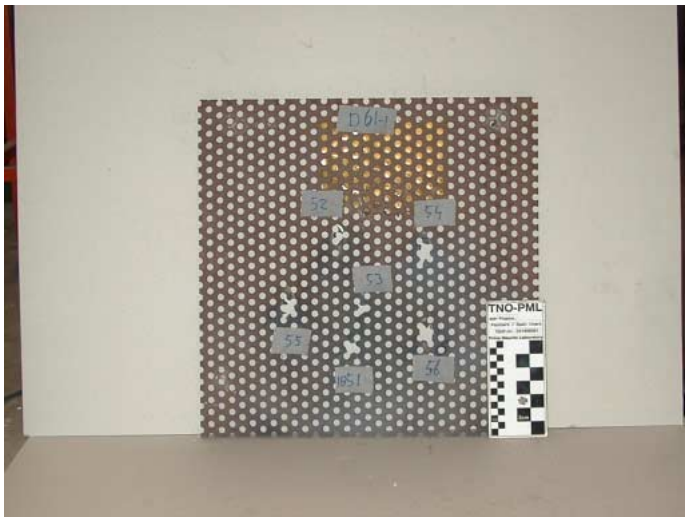

Fig. 14. Frontside of a plate of MARS-300 perforated, armour configuration 12 (60º NATO).

Fig. 15. Backside of an aluminium plate of armour configuration 12 (60º NATO).

Titanium en Dyneema spall-liner (armour configurations 6 to 8)

The armour configurations consisting of titanium base armour and very hard steel armour (spaced by an airgap) have a considerable lower areal density than comparable armour configurations with aluminium base armour (armour configurations 1 to 5). Comparing targets 6 and 3, both with the same ARMOX-600S frontplate, the derived and estimated mass efficiency of titanium is 1.65 and right in-between the values ranging from 1.5 to 1.8 as reported in various references. Note however that no semi-infinite targets were used.

Because titanium armour shows considerably more spalling than aluminium, armour configuration 7 has been supplied with a thin Dyneema spall-liner bolted at the inside of the titanium plate (see figure 19). Except for the Dyneema spall-liner, armour configurations 6 and 7 are he same. The primary function of the spall-liner is to intercept armour debris and projectile parts. Besides, it is known from experience that for a tightly dimensioned armour (close perforation at muzzle velocity, close stop at a lower velocity) application of a thin spall-liner can increase the ballistic performance considerably compared to the modest increase in areal density by adding a lightweight spall-liner.

The thin Dyneema spall-liner is well capable of intercepting both the armour debris and the projectile parts. Figure 16 shows an Imacon recording of target 6 (ARMOX-600S plus titanium without spall-liner) where the spall cloud is visible. Figure 17 depicts the belonging titanium plate (backside). Figure 18 shows an Imacon recording of target 7 (similar to target 6 plus spall-liner) where the Dyneema liner catches the armour debris and projectile parts. Figure 19 depicts the belonging Dyneema plate (backside). The incendiary tip of the projectile causes the bright flash in the Imacon recordings.

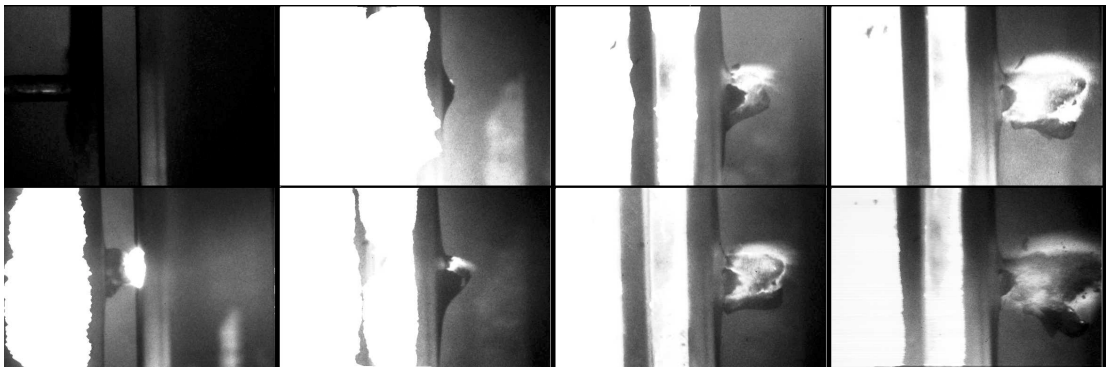

1	3	5	7
2	4	6	8

Fig.16. Imacon recording of target 6 (ARMOX-600S / airgap / titanium), impact velocity 927 m/sec, timeframe per recording 40 µsec, exposure 1 µsec.

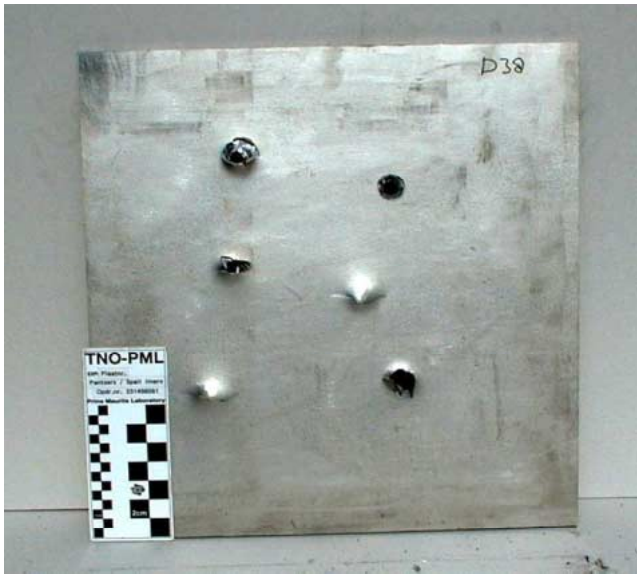

Fig. 17. Backside of titanium plate (target 6).

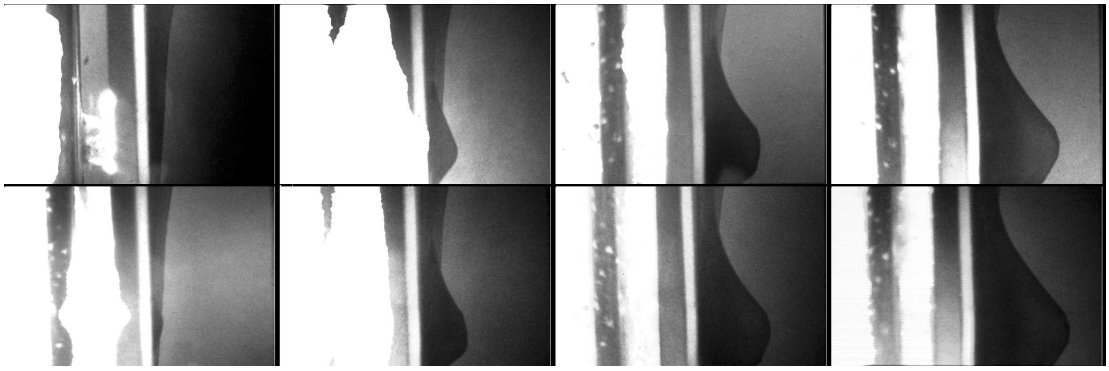

1	3	5	7
2	4	6	8

Fig. 18. Imacon recording of target 7 (similar to target 6 plus Dyneema), impact velocity 992 m/sec, timeframe per recording 40 μsec, exposure 1 μsec.

Fig. 19. Backside of Dyneema plate (target 7).

LIBA (armour configurations 9 and 10)

For normal impact, the LIBA target (armour configuration 9) has a considerable lower areal density than the targets involving metallic front plates (armour configurations 1, 2, 3, 11, 6 and 7). For normal impact, the estimated mass efficiency of the applied LIBA plate itself is 3 for the specific threat in question (14.5 mm AP-I B32). Note however that no semi-infinite targets were used.

For 60º NATO impact angle, no clear profit in areal density relative to armour configurations comprising steel armour plates can be distinguished (compare armour

configuration 10 to 4, 5, 8 and 12). Obviously, armour configuration 10 has not yet been optimized; better results can be expected because of the high mass efficiency of LIBA at normal impact.
Figure 20 gives a picture showing the composition of a LIBA plate (armour configuration 9). Figure 21 indicates the hole sizes and possible multihit capacity of LIBA against 14.5 mm AP (armour configuration 10, 60º NATO).

Fig. 20. Part of a LIBA plate of armour configuration 9, showing its composition.

Fig. 21. Frontside of a LIBA plate of armour configuration 10, impacted at 60º NATO.

DIMOX-AS, Type 112 (armour configuration 13)
For the DIMOX tiles, consisting of SiC, Al_2O_3 and aluminium, only a V50 has been established for normal impact. The DIMOX tiles should have a much better multihit capacity than monolitic ceramic tiles, but they exhibit the same one-shot performance. In contrast to monolitic tiles the DIMOX tiles do not pulverize (as in figure 23), but break up into large pieces (see figure 22). It is quite possible that the applied DIMOX

tiles are too thin against the 14.5 mm AP-I B32 projectile; the areal density of armour configuration 13 is less than 40% of the areal density of RHA required to stop the same threat. Thicker DIMOX tiles will probably exhibit a much better multihit capacity, albeit at the expense of a larger areal density. Moreover, given a better multihit capacity than monolitic tiles, DIMOX could be applied as a larger plate instead of 100 x 100 mm square tiles, resulting in a smaller chance of hitting the DIMOX near an edge or near a corner.

Fig. 22. Impacted DIMOX tile (armour configuration 13).

Ceramic tiles (SiC and Al_2O_3) on aluminium

It was the intention to incorporate SiC ceramic tiles on aluminium in figure 6 for comparing their ratio of V99 and areal density to the other tested armour configurations. However, the armour configuration (areal density: around 48% of RHA for normal impact) could not be perforated. In fact, inspection learned that the underlying aluminium armour was not even damaged. Figure 23 shows a picture of a SiC tile (black) hit near a tile edge and surrounded by Al_2O_3 tiles (white). Obviously, the combination of SiC tiles and aluminium armour will have a very favourable ratio of V99 and areal density compared to the other armour configurations.

Fig. 23. SiC tile (black), leaving the underlying aluminium armour undamaged.

Because of the good results with SiC tiles, as a reference we also did some tests on the much cheaper 'common' Al_2O_3 tiles on the same aluminium armour (areal density: around 51% of RHA for normal impact). Again, the armour configuration could not be perforated, but the aluminium base armour did suffer some damage. Figure 24 shows two damaged Al_2O_3 tiles, figure 25 shows the backside of the belonging aluminium backing. The shot at the tile at the right in figure 24 results in a bulge in the aluminium backing at the left in figure 25. The other shot results only in some paint removal from the backside of the aluminium. Obviously, the combination of Al_2O_3 tiles and aluminium armour will have a much better ratio of V99 and areal density than the metallic armour configurations and may even have a similar or better ratio compared to the armour configurations with LIBA. The latter however has a much better multihit capacity than ceramic tiles.

Fig. 24. 'Common' Al_2O_3 tiles on aluminium, stopping 14.5 mm AP-I B32.

Fig. 25. Backside of the aluminium armour, backing the Al_2O_3 tiles of figure 24.

7. Accuracy and reliability

The accuracy and reliability of the results and their translation into threshold velocities or estimated stopping probabilities are influenced by a number of factors. The most important factors are:

- Bending of armour plates and reduction of airgap after the first impact
- The influence of the spinrate of the projectile
- Spread in behaviour of the ammunition
- Bending of aluminium plates backing LIBA targets.

The impacted armour plates show some bending, causing a reduction of the air gap in spaced targets in the vicinity of the impact position and causing the next impact in the direct vicinity to have a slightly different impact angle. The possible influence on the results has been minimized by re-aligning the target configuration after each shot (unless the bending is too large, then a new target must be used) and by choosing the impact positions far enough from one another.

Because the shooting distance is simulated by removing some gunpowder from the cartridge, the spinrate of the projectile during the experiments is different than in real situations. The possible influence on the results can be checked using computer simulations, e.g. the hydrocode Autodyn. This has yet to be done.

The used Russian 14.5 mm AP ammunition shows a less reproducible behaviour than for instance the customary NATO small-calibre ammunition. Sometimes the steel core breaks up when impacting a certain target at a certain impact velocity, the next time it does not break up under the same conditions. The influence of this spread in behaviour on the establishment of threshold velocities will decrease with an increasing number of shots.

The results for LIBA targets (armour configurations 9 and 10) can be negatively influenced after several impacts because of bending of the underlying aluminium plates on which he LIBA is clamped, possibly causing local loss of direct support of the LIBA by the aluminium backing. However, it is not feasible to use each target for only one or two shots. After each shot, the target was inspected and, if necessary, the LIBA and aluminium plates were dismounted and again mounted to the frame and fixed to one another by screw clamps and quick-acting clamps.

It can be disputed whether the chosen sizes of the airgaps are optimal against 14.5 mm AP. The smallest airgaps may even be useless for these projectiles (but may be useful against smaller calibres). This could be elaborated using computer simulations with the available experimental results as a reference.
In a similar way, it can be disputed whether the chosen armour configurations are optimal against 14.5 mm AP. Again, computer simulations can prevent the need for an additional and non-feasible number of experiments by varying parameters like plate thickness and airgap, material properties and material order at will, based on reference simulations validated by experiments.

8. Conclusions and recommendation

For normal impact and for 99% stopping probability (V99 threshold velocity), the areal density ranges from less than 45% (ceramic pellets in a rubber matrix, backed by aluminium) to around 60% (very hard steel plus aluminium) of the areal density of RHA required to stop the threat (14.5 mm AP-I B32). For 60º NATO impact angle, the areal density ranges from around 50% (very hard steel plus titanium) to over 60% (very hard steel plus aluminium).

Application of a thin polyethylene fibre spall-liner at the inside of a titanium base armour shows a large increase in the V99 threshold velocity (around 100 m/sec) at the expense of only a slight increase in areal density of the armour configuration (around 3%).

The areal densities of the armour configurations of comparable stopping capacity decrease from very hard steel and perforated very hard steel via very hard steel in front of titanium base armour to ceramic pellets in a rubber matrix as outer layer. Although not enough experiments have yet been performed to establish their threshold velocities, experimental results so far indicate that silicium carbide ceramic tiles and even common alumina ceramic tiles adhesively bonded to aluminium base armour will result in smaller areal densities than with the materials mentioned above. However, these ceramic tiles will have a much lower multihit capacity than ceramic pellets in a rubber matrix.

For ceramic matrix composites backed by aluminium only the V50 has been established for normal impact. This armour configuration has a low areal density: less than 40% of the areal density of RHA required to stop the threat (14.5 mm AP-I B32). The multihit capacity however is quite poor, probably because of a too small tile thickness.

Recommendation

Until now cost has not been an issue. This research has focussed on technical possibilities. For practical reasons, one should try to incorporate cost as well. Unfortunately, it is very difficult to obtain reliable and realistic cost information on the newer ballistic materials that have not yet gone into (large) series production. If one would dispose of such information (cost per kg), the results depicted as a graph of the threshold velocity as a function of areal density (kg/m^2) (see figures 6 and 7) could be translated into the threshold velocity as a function of areal cost ($cost/m^2$).

References

[1] Numbers originating from the US National Ground Intelligence Center (NGIC), see Jane's IDR 7/1999, p. 37.

[2] Cohen, M., Israeli, A., ***Composite armor panel and manufacturing method thereof***, European Patent Specification EP 0 843 149 B1, date of publication and mention of the grant of the patent: 26.08.1998.

[3] Kneubuehl, B.P., Improved test procedure for body armour. Statistical base and evaluation program, Personal Armour Systems Symposium 1996, pp. 287-294, 3-6 September 1996, Colchester, United Kingdom.

Appendix A. Mass efficiency

The higher the mass efficiency E_m of a certain armour material the less weight the ballistic protection per unit of area will cost. RHA (Rolled Homogeneous Armour) serves as a reference ($E_m = 1$). E_m is defined as follows:

$$E_m = \frac{\rho_s \cdot p_{ref}}{\rho_A \cdot p_A}$$

ρ_s:	specific density of RHA	[g/cm^3]
ρ_A:	specific density of material A	[g/cm^3]
p_{ref}:	depth of penetration in semi-infinite RHA	[mm]
p_A:	depth of penetration in semi-infinite material A	[mm]

Appendix B. Armour configurations

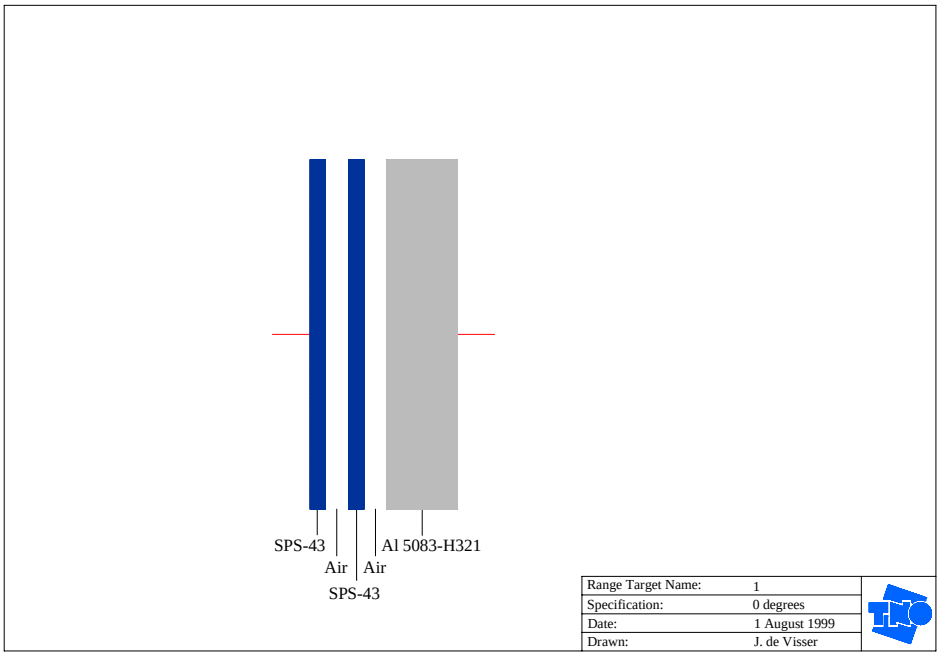

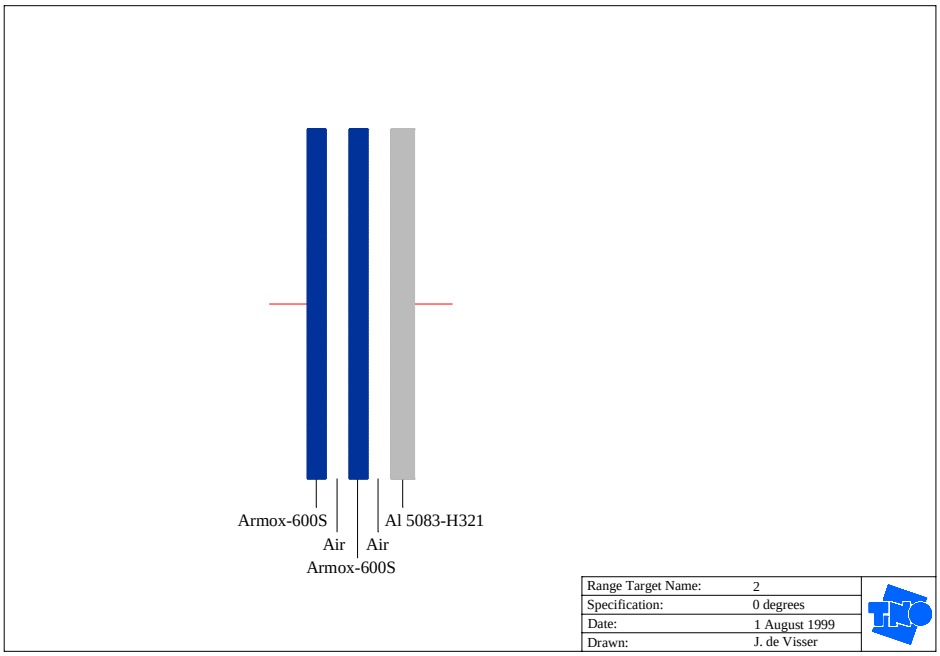

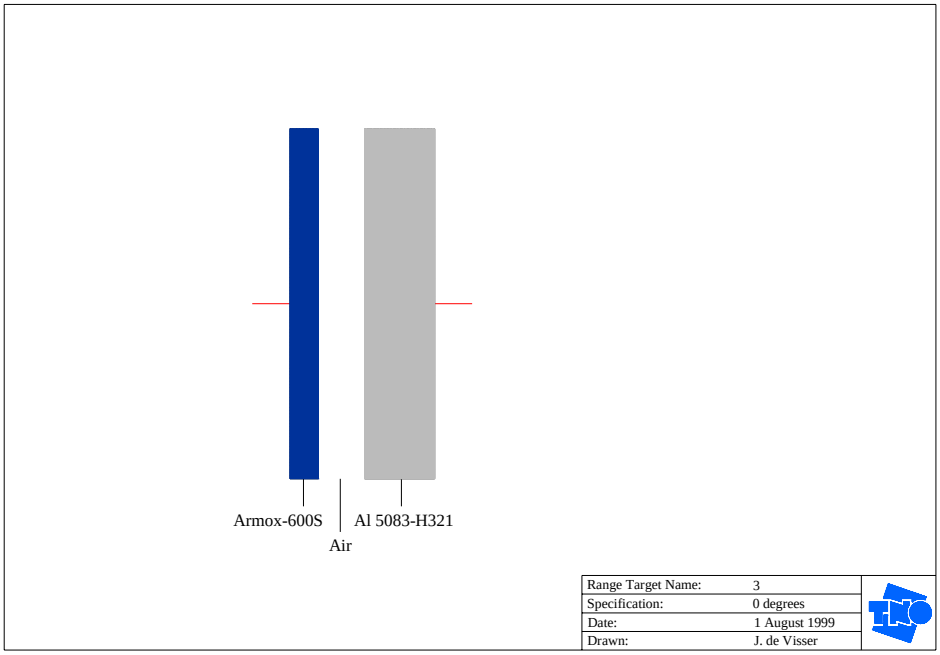

Range Target Name:	3
Specification:	0 degrees
Date:	1 August 1999
Drawn:	J. de Visser

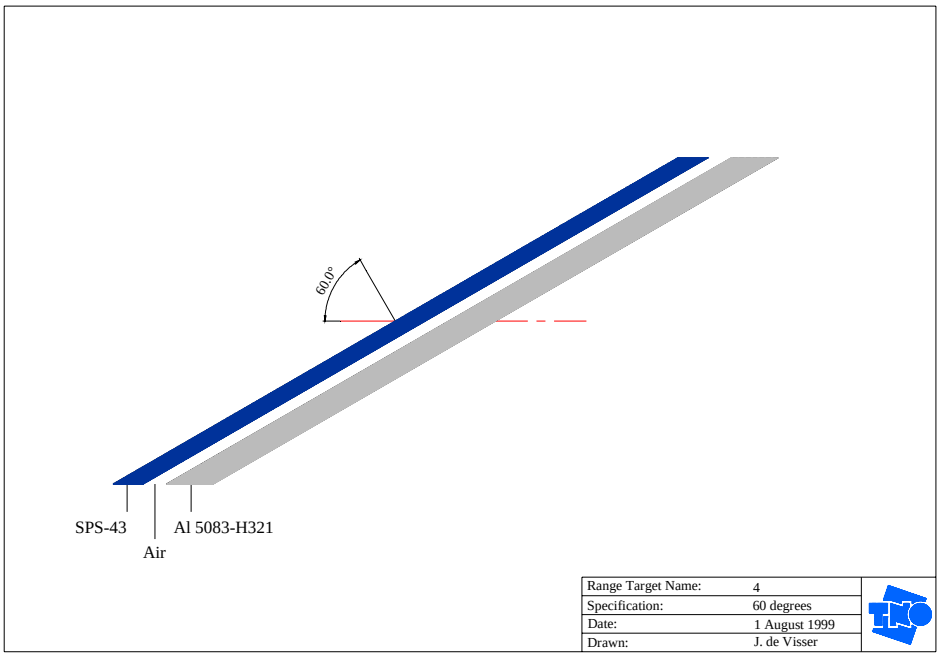

Range Target Name:	4
Specification:	60 degrees
Date:	1 August 1999
Drawn:	J. de Visser

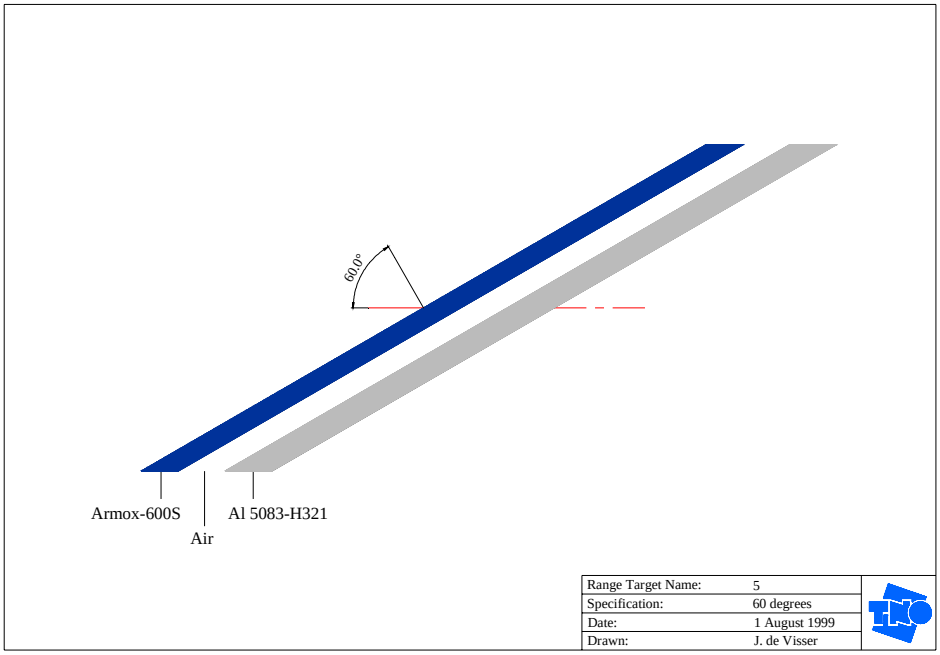

Range Target Name:	5
Specification:	60 degrees
Date:	1 August 1999
Drawn:	J. de Visser

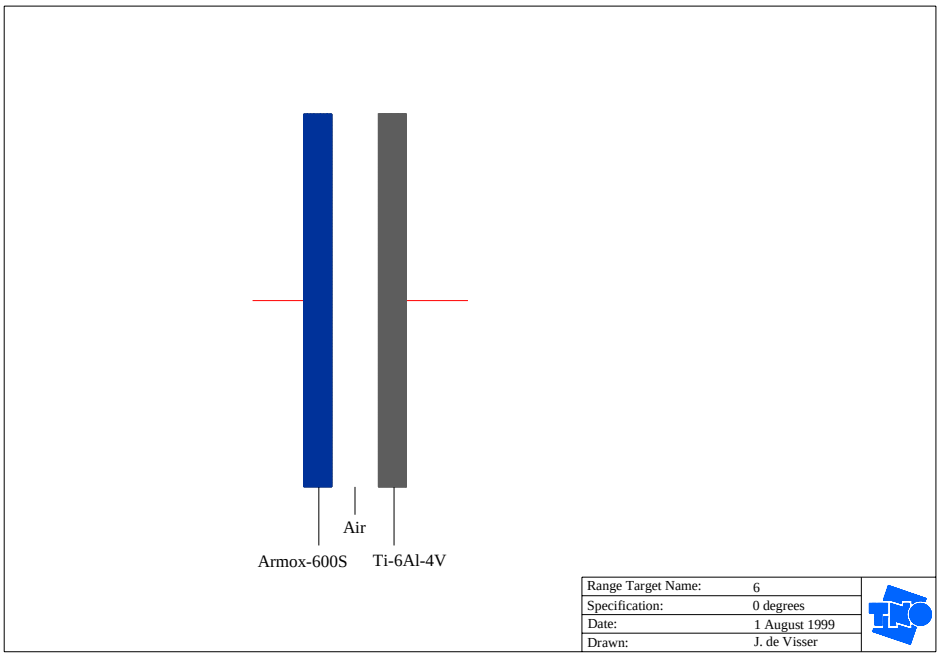

Range Target Name:	6
Specification:	0 degrees
Date:	1 August 1999
Drawn:	J. de Visser

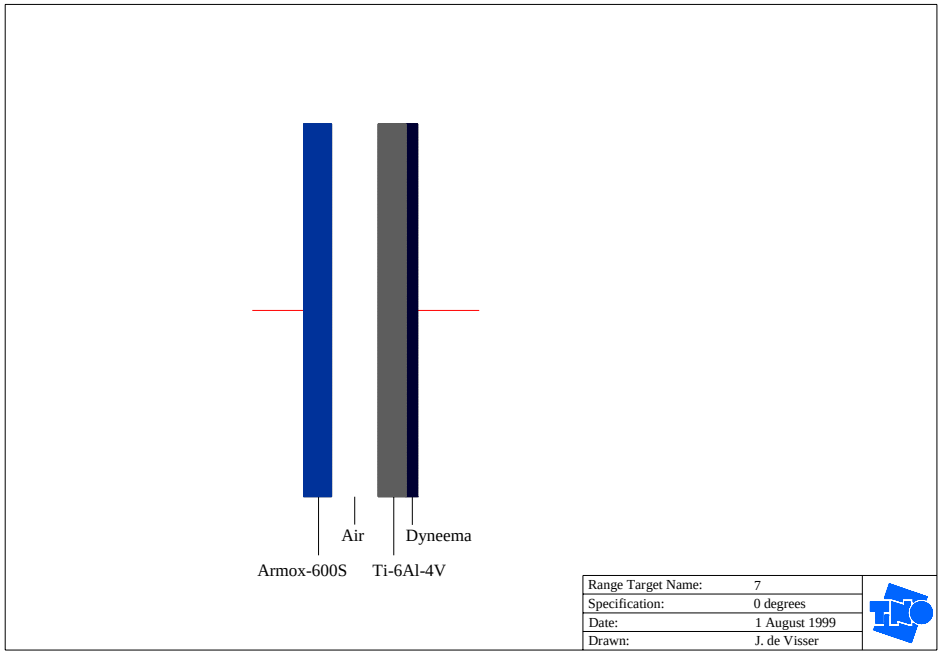

Range Target Name:	7
Specification:	0 degrees
Date:	1 August 1999
Drawn:	J. de Visser

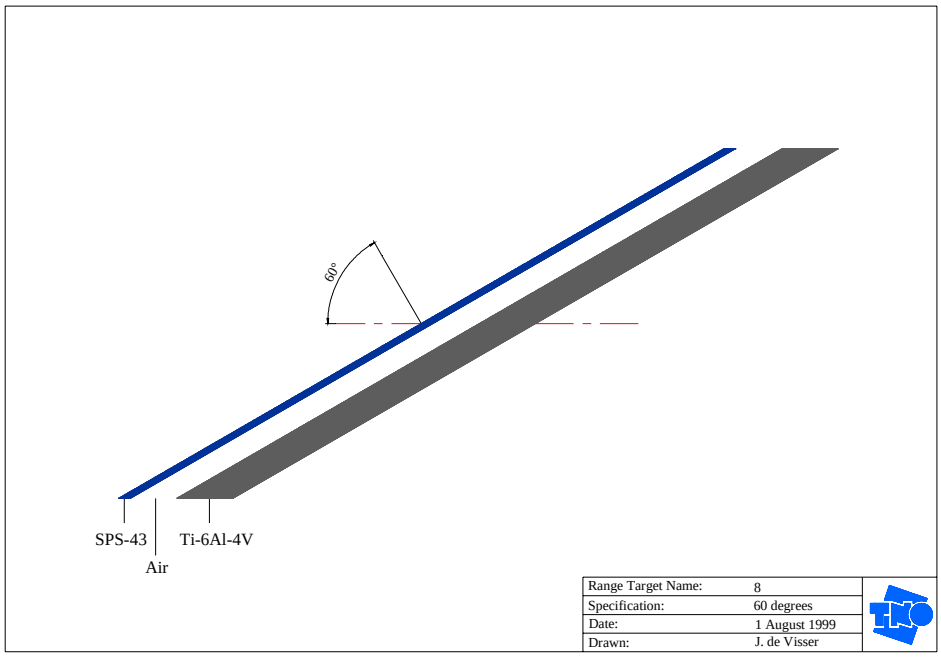

Range Target Name:	8
Specification:	60 degrees
Date:	1 August 1999
Drawn:	J. de Visser

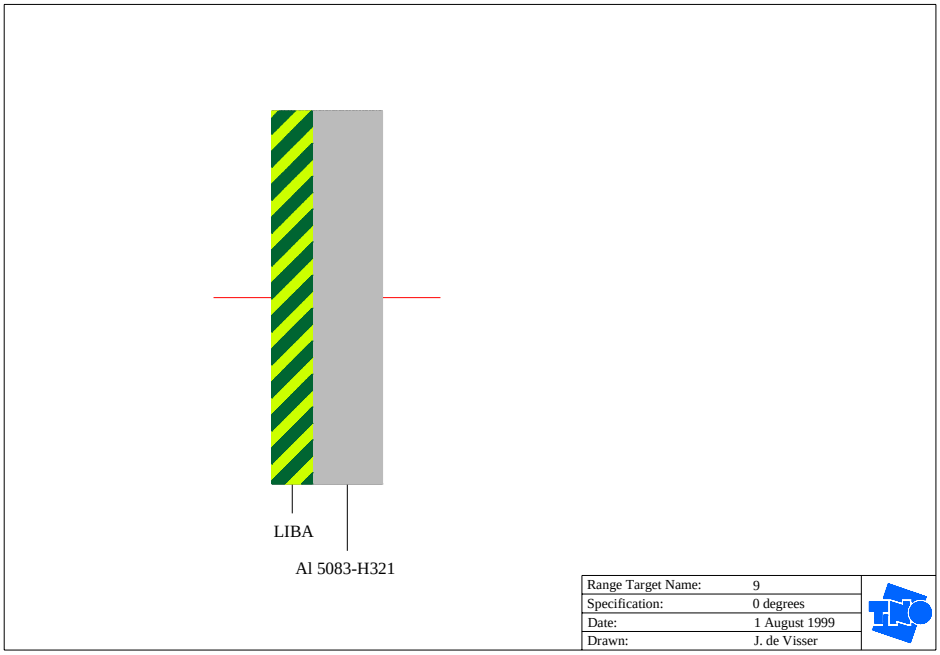
LIBA
Al 5083-H321
Range Target Name: 9
Specification: 0 degrees
Date: 1 August 1999
Drawn: J. de Visser

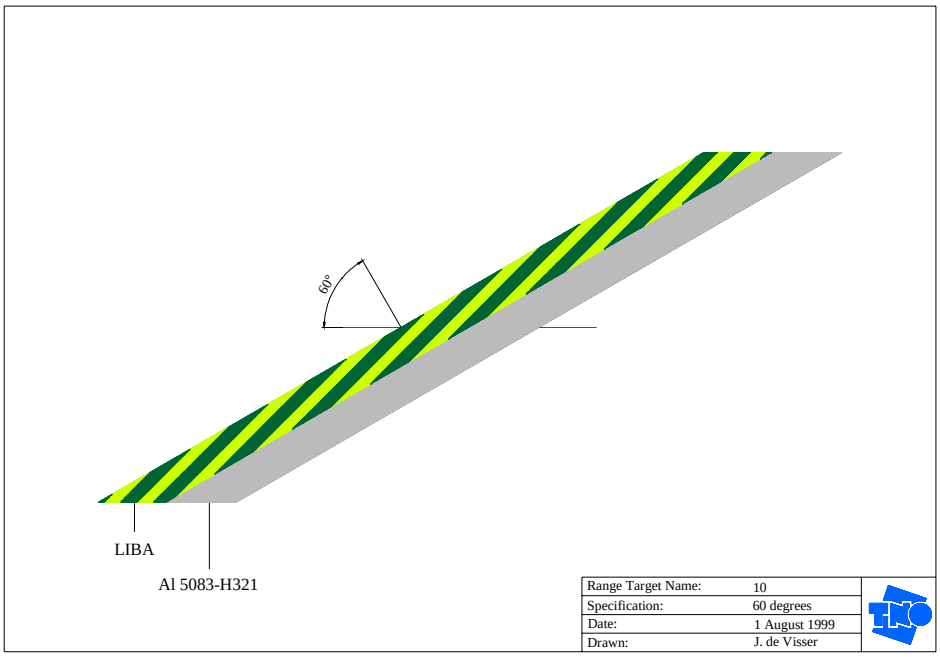
60°
LIBA
Al 5083-H321
Range Target Name: 10
Specification: 60 degrees
Date: 1 August 1999
Drawn: J. de Visser

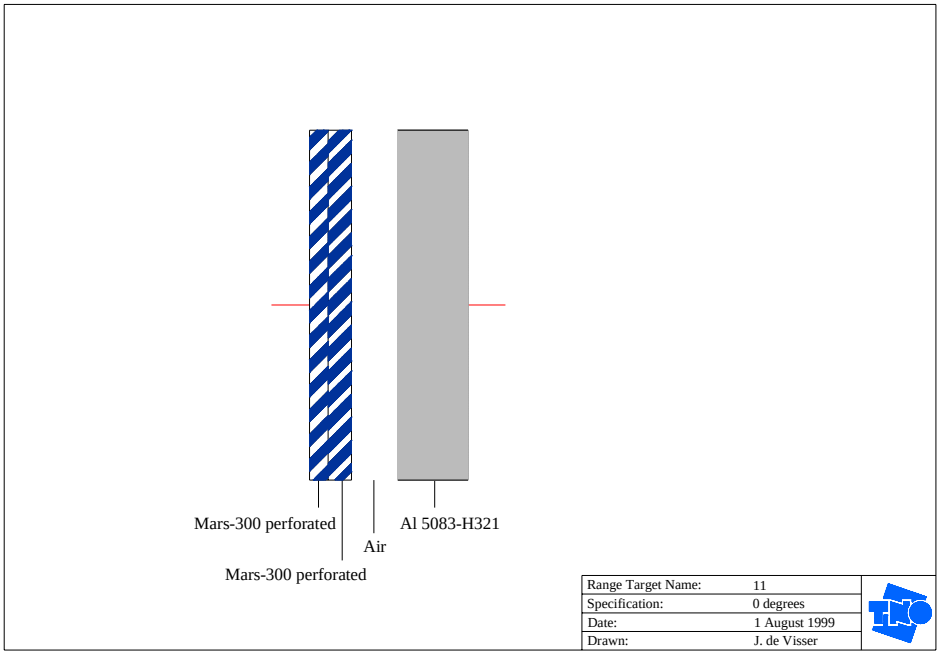

Range Target Name:	11
Specification:	0 degrees
Date:	1 August 1999
Drawn:	J. de Visser

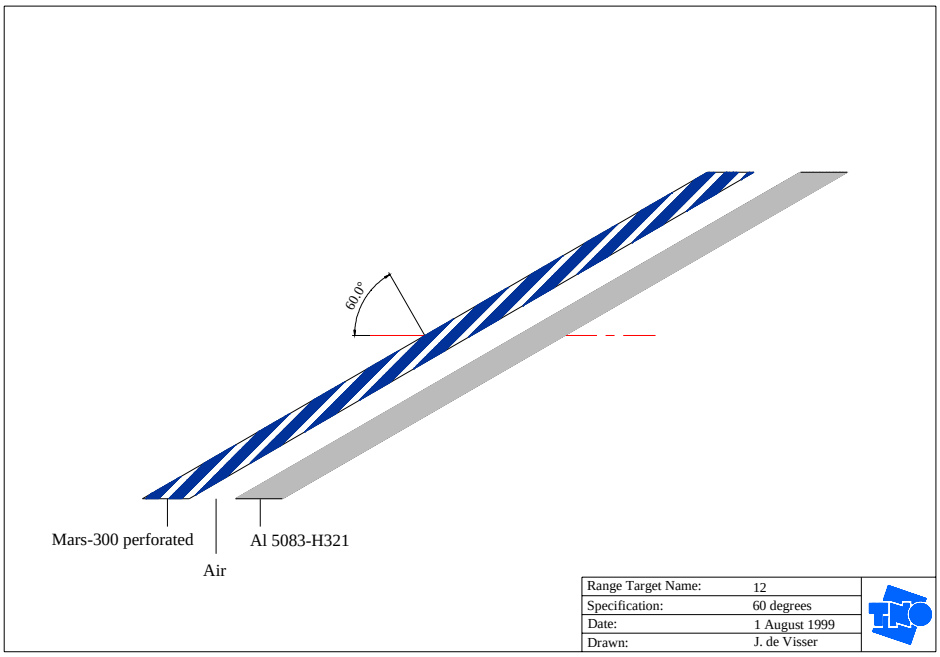

Range Target Name:	12
Specification:	60 degrees
Date:	1 August 1999
Drawn:	J. de Visser

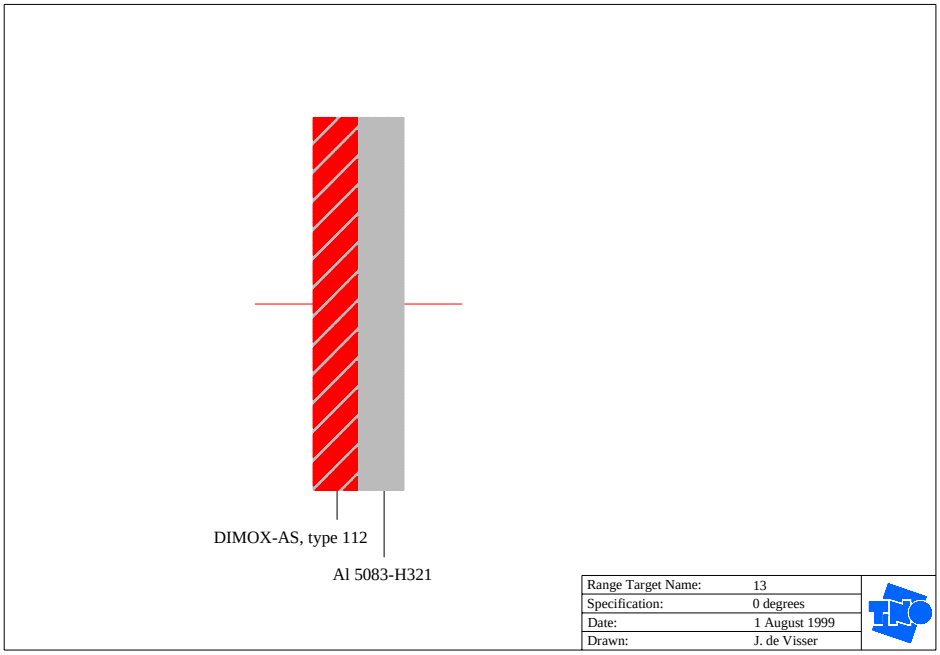
DIMOX-AS, type 112
Al 5083-H321
Range Target Name: 13
Specification: 0 degrees
Date: 1 August 1999
Drawn: J. de Visser